# Modelling strain distributions in ion-implanted magnetic bubble materials

B. E. MacNeal and V. S. Speriosu [a)]
*Rockwell International Corporation, 3370 Miraloma Avenue, Anaheim, California 92803*

(Received 24 November 1980; accepted for publication 6 March 1981)

The detailed properties of strain distributions in $Ne^+$, $B^+$, and $He^+$ implanted magnetic bubble garnet materials are accounted for by calculating the nuclear energy loss as a function of depth. The calculation is based on stopped ion distributions for ZnS, with suitable corrections made for differences in material density. The constant of proportionality $K$ between strain and nuclear energy loss, and the density ratio $l$ are determined for each ion by comparing calculated strain distributions with experimental results obtained previously using an x-ray diffraction technique. It is found that $K$ is roughly the same for all three ions, $0.016 \pm 0.003$ $(eV/Å^3)^{-1}$, and that the average value $l = 0.79 \pm 0.08$ is consistent with the actual density ratio $l = 0.72$. Good agreement is found in additional examples of both single and multiple implants ($\pm$ 10% relative error). Finally, a procedure for selecting the incident energies and dosages required to produce a uniformly strained layer for bubble device applications is described, and then demonstrated by achieving a 0.4-$\mu$m-thick layer with $(1.07 \pm 0.09)$% strain, using a double $B^+$ implant.

PACS numbers: 61.10.Fr, 75.70.Kw, 61.70.Tm

## INTRODUCTION

Ion implantation has been used for some time to make magnetic bubble devices.[1] Damage is produced when incoming ions collide with nuclei and dislodge atoms from their normal positions. Because the lattice in these thin-film, single-crystal garnet materials is constrained by the substrate, the lattice only expands perpendicular to the film plane. The resulting average strain has been found,[2] to be roughly proportional to the energy lost during nuclear collisions. This strain changes the sign of the perpendicular magnetic anisotropy normally found in bubble materials, and the magnetization reorients into the film plane. An independent set of in-plane domains is formed in the implanted layer. The boundaries between these domains, charged walls, attract bubbles in the underlying layer and are responsible for propagation. For optimum performance, the strain should be uniform through the thickness of the implanted layer. In order to achieve such uniform implants, an accurate model capable of predicting the detailed properties of strain distributions as a function of dosage, incident energy, and implant species is required. Such a model is the subject of the present work.

The damage produced by ion implantation has been calculated using a variety of techniques.[3] In Monte Carlo calculations the behavior of a single ion is studied as it penetrates the material. Data regarding the energy lost during nuclear collision are accumulated for a number of ions until the desired statistical accuracy is achieved. In the LSS theory[4] the statistical moments of the nuclear energy loss distributions are obtained by solving the transport equations. Both methods involve a large amount of computation and therefore are not suitable for use as a guide in selecting implantation parameters.

The method presented here, which is similar to that used by Ju *et al.*[5] uses the tabulated properties of LSS stopped ion distributions[6] to obtain strain distributions with a minimal amount of computation. Results are compared with distributions obtained previously using an x-ray diffraction technique.[7-9] First, the model is calibrated for $Ne^+$, $B^+$, and $He^+$ implantations by comparing results for single implants. Then, additional examples are used to illustrate the effects of varying incident energy and dosage on the strain distribution. With the good agreement found between calculated and experimental results, the mechanisms responsible for the characteristics of the distributions are inferred from the calculation. Examples of multiple implants involving the same and different species are presented and a procedure for selecting energies and dosages to produce a uniformly strained layer is described.

## EXPERIMENTAL RESULTS

Experimental strain distributions were obtained previously using an x-ray diffraction technique. 2 $\mu$-thick YSmTmCaGeIG bubble materials were implanted with $Ne^+$, $B^+$, and $He^+$, using incident energies up to 200 keV and a dosage rate of 1 $\mu A/cm^2$. The materials were misaligned with respect to the ion beam by 7° in order to avoid channeling. The expanded lattice in the implanted layer produces a series of secondary peaks in CuK$\alpha$ (444) double crystal x-ray diffraction curves. Several curves were obtained after varying amounts of the implanted layer had been removed by chemical etching (nitric acid, 90 °C). Theoretical curves were calculated using a kinematical model of x-ray diffraction for various trial strain and damage distributions and compared with experimental results. The damage distribution characterizes the reflection efficiency at a given depth. The distributions were adjusted until good agreement was achieved for each etching step. The calculated curves are quite sensitive to small changes in the strain distributions, so that the maximum relative uncertainty at any point in the final strain distribution is only about 2%. The relative uncertainty in the damage distribution is much larger, about 20%. In general, the strain and damage distributions were both found to have an asymmetric shape—nonzero at the surface,

[a)]Permanent address: California Institute of Techonology, Pasadena, California, 91125.

 0021-8979/81/063935-06$01.10  

rising to a maximum, then falling rapidly to zero at the bulk interface. The distributions were flatter for heavier ions, and their depth increased with increasing incident energy. The average strain was proportional to total dosage up to about 2% strain. At higher dosages the x-ray signal disappeared owing to the formation of an amorphous layer.

## THEORY

The strain $S$ is obtained by summing nuclear energy loss contributions from ions stopped at different depths. Consider those ions that stop in the depth interval $x'$ to $x' + dx'$. The number of ions stopped in this interval (per unit area) is given by the stopped ion distribution $n(x')dx'$. It is apparent from theoretical range calculations[6] that ion energy decreases at a nearly constant rate with increasing depth. Thus at some other depth, $x < x'$, the ions that stop at $x'$ had an energy $E = E_i[(1 - (x/x')]$, where $E_i$ is the incident energy at the surface, $x = 0$. It is assumed that the strain produced at $x$ by these ions is proportional to the energy lost during nuclear collisions (per unit volume). This energy loss density is given by the loss rate $N(E)$ (per unit distance perpendicular to the film plane), which depends on ion energy, multiplied by the ion flux, $n(x')dx'$. The total strain $S(x)$ is given by an integral over the stopped ion distribution:

$$S(x) = K\int_x^\infty dx' n(x') N[E(x,x')]. \tag{1}$$

In this work the constant $K$ will be determined by comparing $S(x)$ with experimental results. In the case of multiple implants, where different species and/or incident energies are used, strain contributions from different implantation components are additive.

The stopped ion distributions used in Eq. (1) are obtained from their tabulated statistical properties.[6] For heavy ions or low incident energies the distributions can be represented by Gaussian distributions, and only the first two statistical moments, the projected range $R_p$ and straggle $\sigma_p$, are needed. For the cases considered here, the distributions are skewed toward the surface, and the third central moment of $\gamma$ is large (and negative). In this work, all stopped ion distributions are represented by Pearson Type IV functions[10] with the first three moments equal to the tabulated values. The fourth moment $\beta$ is also required to construct the Pearson IV function, but tabulated values are not available. Instead, the experimental relationships, $\beta \simeq 1 + 2\exp(-\gamma)$, found by Holker *et al.*[11] for $B^+$ in amorphous silicon are used; however, it should be noted that this function is not sensitive to particular choices for $\beta$.

Stopped ion distributions are not yet available for bubble materials, so that statistical moments and nuclear energy loss rates calculated for ZnS are used.[6] Because bubble materials are more dense than ZnS, ions do not penetrate as far and both $R_p$ and $\sigma_p$ must be reduced by the density ratio $l$. The nuclear energy loss rate $N(E)$ must be increased by $l^{-1}$, but the dimensionless moments $\gamma$ and $\beta$ remain unchanged. As indicated in deriving Eq. (1), the nuclear loss rate $N$ should be measured perpendicular to the film plane along the projected range $R_p$. Since the tabulated values[6] are measured along the ion path $R$, they must be corrected by the factor $(dR/dR_p)$.

## ANALYSIS AND DISCUSSION

Fitted values for $K$ and $l$ were obtained separately for the three implant species $Ne^+$, $B^+$, and $He^+$, and the results are shown in Figs. 1–3. Single implants were used with the energies and dosages chosen to give roughly the same overall strain and depth. The stopped ion distributions (dashed curves) are shown with arbitrary veritcal scales and no attempt has been made to indicate the actual total dosages. The arrows indicate the average range $R_p$. Using these distributions, the integral in Eq. (1) was evaluated numerically for each case and the results, shown as solid curves, were compared with the x-ray distribution (●). The constant $K$ was chosen to match the peak strain values while $l$ was adjusted to match the depth of the transition region between the implanted layer and the underlying nonimplanted material. The shape of $S(x)$ is governed by $n(x')$ and $N(E)$ and was not adjusted.

The results for a 200-keV/$Ne^+$/$2\times10^{14}$ ions/cm$^2$ implant are shown in Fig. 1. Best agreement was found for the parameter values $K = 0.020\,(\text{eV/Å}^3)^{-1}$ and $l = 0.87$, so that the first four moments of the stopped ion distribution, when adjusted for differences in material density, were $(R_p, \sigma_p, \gamma, \beta) = (0.239\,\mu\text{m}, 0.083\,\mu\text{m}, -0.6, 5)$. It can be seen that excellent agreement is obtained not only for the peak strain and overall depth, but also in the detailed shape of the distribution.

The results for a 150-keV, $1\times10^{15}$ ions/cm$^2$ $B^+$ implant are shown in Fig. 2. Best agreement was found using a lower value of $K$, $0.014\,(\text{eV/Å}^3)^{-1}$, and the fitted value of $l$, 0.71, is much smaller than the value used for $Ne^+$. The first four moments of the stopped ion distribution were $(0.295\,\mu\text{m}, 0.094\,\mu\text{m}, -1.0, 6)$. Again, excellent agreement

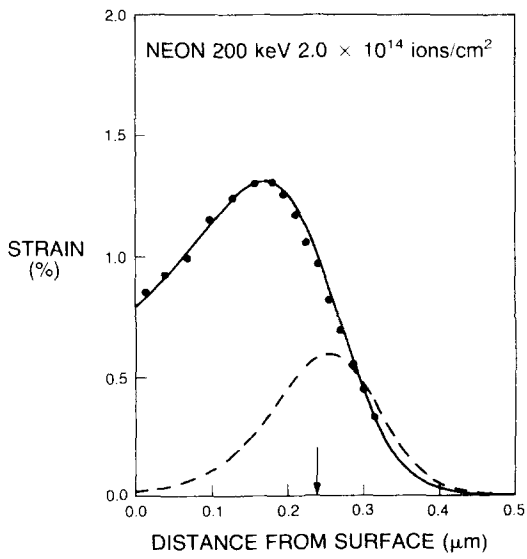


FIG. 1. Calculated (solid) and x-ray (dots) strain distribution (%) as a function of depth below the surface ($\mu$m) for the single implant, 200 keV/$Ne^+$/$2\times10^{14}$ ions/cm$^2$. The stopped ion distribution is indicated by a dashed curve and the arrow indicates the average projected range $R_p$.

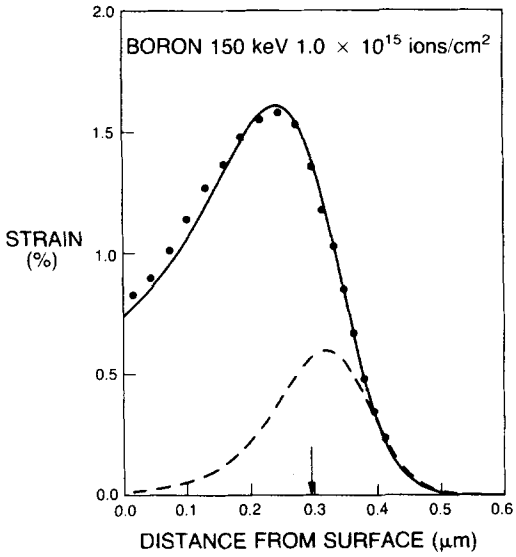


FIG. 2. Calculated (solid) and x-ray (dots) strain distributions (%) as a function of depth ($\mu$m) for the single implant, 150 keV/$B^+$/$1\times10^{15}$ ions/cm$^2$.

found between the detailed shapes of the calculated and x-ray curves.

Figure 3 shows the results for the implant 60 keV/$He^+$/$5.5\times10^{15}$ ions/cm$^2$. The fitted value of $K$, 0.014 (eV/Å$^3$)$^{-1}$, is the same as with $B^+$, and the value for $l$, 0.80, lies between the two previous values. The first four moments fo the stopped ion distribution were (0.265 $\mu$m, 0.082 $\mu$m, − 1.2, 8). It can be seen that the agreement in the distribution is not as good as in the two previous cases because the calculation underestimates the surface strain by a factor of 0.8. This discrepancy may be due to annealing during implantation, with most of the annealing taking place near the strain peak.

The average value, $K = 0.016 \pm 0.003$ (eV/Å$^3$)$^{-1}$, obtained here for $Ne^+$, $B^+$, and $He^+$ implants is somewhat higher than the estimate given by North and Wolfe[2] for 300-keV $He^+$ implants, $K \approx 0.01$ (eV/Å$^3$)$^{-1}$; however, their strain values tend to saturate with increasing dosage possibly owing to annealing during implantation. This would account for the lower value of $K$. There is considerable scatter in the fitted values of $l$, but the average value, $l = 0.79 \pm 0.08$, is close to the value obtained from the ratio of material densities, $l = 0.72$.

Attempts have been made to calculate strain distributions for $H^+$ implants. The calculated distributions do not agree with the detailed shape of the x-ray results, especially near the surface where 30% disagreement was often found. This may be due to annealing during implantation, because the value of $K$ obtained for a given component varies substantially depending on whether it is used by itself or as a part of a multiple implant. Work is continuing in this area.

The single implants shown in Figs. 1–3 all have the same characteristic shape, which results from two competing effects: (i) the increase in $N(E)$ with decreasing energy, and (ii) the decrease in the number of penetrating ions with increasing depth. Most of the ions pass through the surface region, but their energy is relatively high and the resulting energy loss and strain are low. As the ions lose energy with increasing depth, the damage and strain increase, but at the same time fewer ions penetrate so the strain reaches a maximum near $R_p - \sigma_p$. Beyond $R_p$, the number of penetrating ions decreases rapidly and the strain decreases, following the deep edge of the stopped ion distribution.

The effects of decreased dosage on the strain distribution can be seen in Fig. 4. For this single $Ne^+$ implant, the incident energy, 200 keV, was the same as in Fig. 1 but the dosage was reduced by more than a factor of 3, to $6\times10^{13}$ ions/cm$^2$. In this and all subsequent examples, the fitted values of $K$ and $l$ obtained previously were used to calculate $S(x)$, and no further adjustments have been made. The stopped ion distribution used here is the same as in Fig. 1. The good agreement shown here confirms the assumption made earlier in deriving Eq. (1) that the strain at any point in

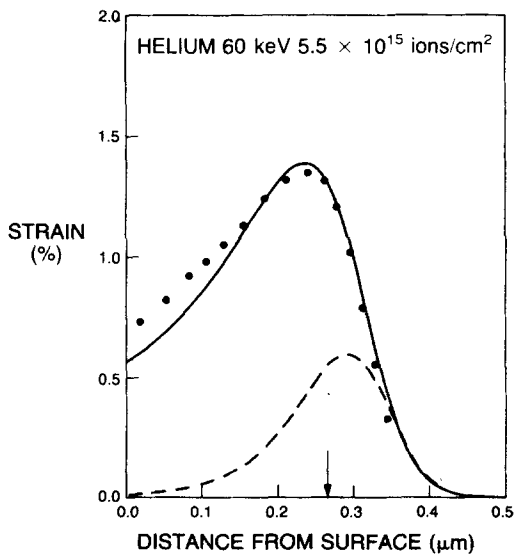


FIG. 3. Calculated (solid) and x-ray (dots) strain distribution (%) as a function of depth ($\mu$m) for the single implant, 60 keV/$He^+$/$5.5\times10^{15}$ ions/cm$^2$.

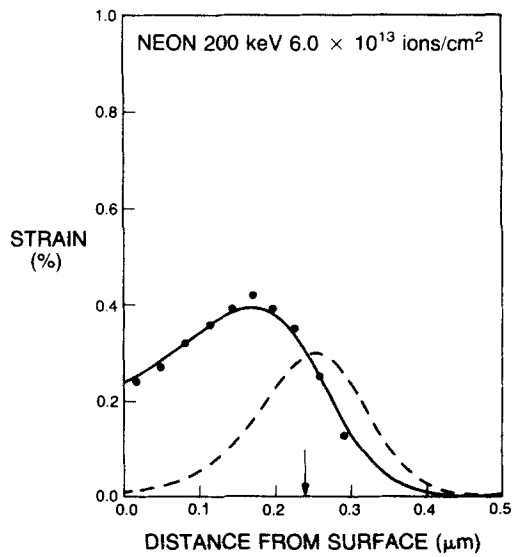


FIG. 4. Calculated (solid) and x-ray (dots) strain distribution (%) as a function of depth ($\mu$m) for the single implant, 200 keV/$Ne^+$/$6\times10^{13}$ ions/cm$^2$.

the distribution is strictly proportional to the total dosage.

The effects of decreased incident energy can be seen in the $Ne^+$ implant shown in Fig. 5. The dosage used here, $6\times10^{13}$ ions/cm$^2$, was the same as in Fig. 4, but the incident energy was reduced to 120 keV. The statistical moments of $n(x')$ are (0.142 $\mu$m, 0.058 $\mu$m, $-$ 0.4, 4). The agreement between the x-ray and calculated distributions shown here is not as good as in previous examples, but it is still within 0.1% strain at each point. The main effect of decreasing $E_i$ is to reduce the overall thickness of the implanted layer, as might be expected. In addition, because $E_i$ is smaller, $N(E)$ is increased and the resulting strain is higher, with largest increase occurring near the surface. Hence, in addition to producing a thinner implant, reducing the incident energy also produces a flatter distribution with somewhat higher strain.

An example of multiple implantation using the same species, $Ne^+$, is shown in Fig. 6. Here, the 200- and 120-keV implants described earlier have been superimposed with a shallow, 50-keV, $6\times10^{13}$ ions/cm$^2$ implant. The statistical moments of the shallow implant are (0.057 $\mu$m, 0.029 $\mu$m, $-$ 0.07, 3.2). Excellent agreement between the x-ray and calculated distributions can be seen except for one point at the surface. The reason for this discrepancy, which has been found in another example of shallow $Ne^+$ implants, is unknown at the present time. The strategy followed here is not suitable for bubble device applications. By maintaining a constant dosage, the strain increases with decreasing energy. As a result, the strain distribution is not uniform, but decreases almost linearly with increasing depth. In addition, the stopped ion distributions have been placed close together in relation to their width, so that strain peaks from individual components cannot be identified. It is clear from this example that in order to achieve a uniform strain profile, the dosage of the two shallower implants should be reduced.

The example shown in Fig. 7, a double $Ne^+$-$He^+$ implant, is more typical of bubble device implants. Here, a 140-keV, $8\times10^{15}$ ions/cm$^2$ $He^+$ implant was used to produce the deep portion of the layer and a 200-keV, $1\times10^{14}$ ions/cm$^2$ $Ne^+$ implant was used to produce the shallow portion. The statistical moments of the $He^+$ implant are (0.523 $\mu$m, 0.109 $\mu$m, $-$ 1.8, 13). The good agreement shown between the x-ray and calculated strain distributions indicates that contributions from individual components involving different species are additive. This implant is more uniform than the previous example; but by only using two implants to produce this rather thick layer, the individual components do not overlap sufficiently and two distinct peaks can be seen. A third component could be used to produce a more uniform implant.

A method for selecting those energies and dosages that will produce a uniform implanted layer is suggested by these results. The energy of the first component is chosen so that the deep edge of its stopped ion distribution, roughly at $^1R_p$,

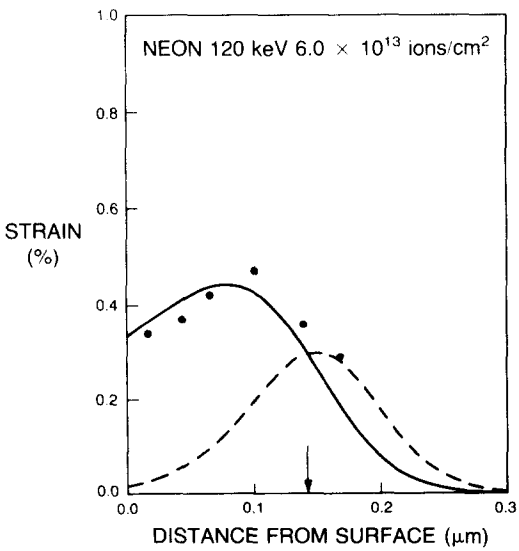


FIG. 5. Calculated (solid) and x-ray (dots) strain distributions (%) as a function of depth ($\mu$m) for the single implant, 120 keV/$Ne^+$/$6\times10^{13}$ ions/cm$^2$.

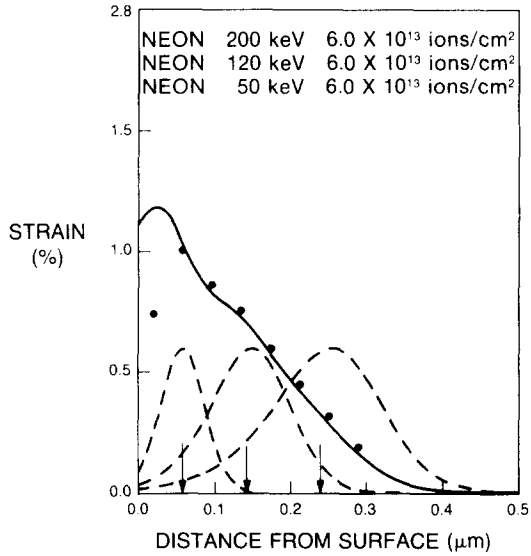


FIG. 6. Calculated (solid) and x-ray (dots) strain distributions (%) as a function of depth ($\mu$m) for the triple implant, 200 keV/$Ne^+$/$6\times10^{13}$ ions/cm$^2$ plus 120 keV/$Ne^+$/$6\times10^{13}$ ions/cm$^2$ plus 50 keV/$Ne^+$/$6\times10^{13}$ ions/cm$^2$.

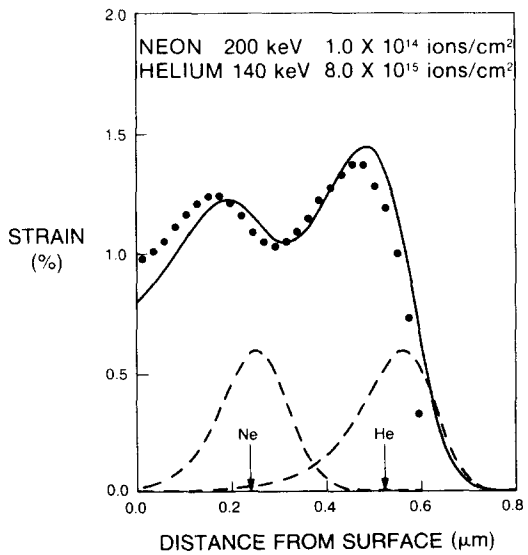


FIG. 7. Calculated (solid) and x-ray (dots) strain distributions (%) as a function of depth ($\mu$m) for the double implant, 200 keV/$Ne^+$/$1\times10^{14}$ ions/cm$^2$ plus 140 keV/$He^+$/$8\times10^{15}$ ions/cm$^2$.

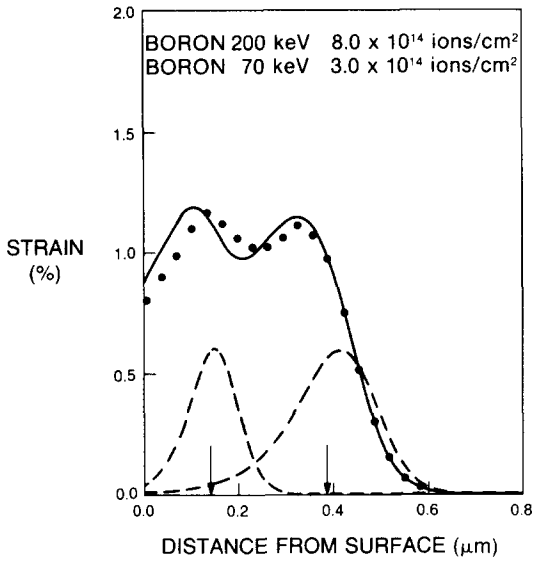


FIG. 8. Calculated (solid) and x-ray (dots) strain distributions (%) as a function of depth ($\mu$m) for the double implant, 200 keV/$B^+$/$8\times10^{14}$ ions/cm$^2$ plus 70 keV/$B^+$/$3\times10^{14}$ ions/cm$^2$. The strain in the implanted layer (less than 0.4$\mu$m depth) is (1.07 $\pm$ 0.09)%.

corresponds to the desired total thickness. The strain distribution is then calculated and the dosage $^1D$ is adjusted so that the peak strain is slightly higher than the desired uniform value. The energy of the second components, which may use the same or a different species, is then selected to give the desired amount of overlap, typically, $(^1\sigma_p + {}^2\sigma_p) < {}^1R_p - {}^2R_p < 2(^1\sigma_p + {}^2\sigma_p)$. The resulting strain distribution is calculated by adding contributions from the first and second components and $^2D$ is adjusted so that the two strain peaks are equal. Additional components are added in the same manner unitl the last component reaches the film surface. The resulting implanted layer will be fairly uniform with the desired strain and depth characteristics. More components spaced closer together can be used to produce a more uniform layer; however, as the number of components increases the inaccuracies of the model accumulate and it may not be possible to accurately predict the distribution near the film surface.

The double $B^+$ shown in Fig. 8 was designed using this procedure. The 200-keV implant, with moments (0.384 $\mu$m,

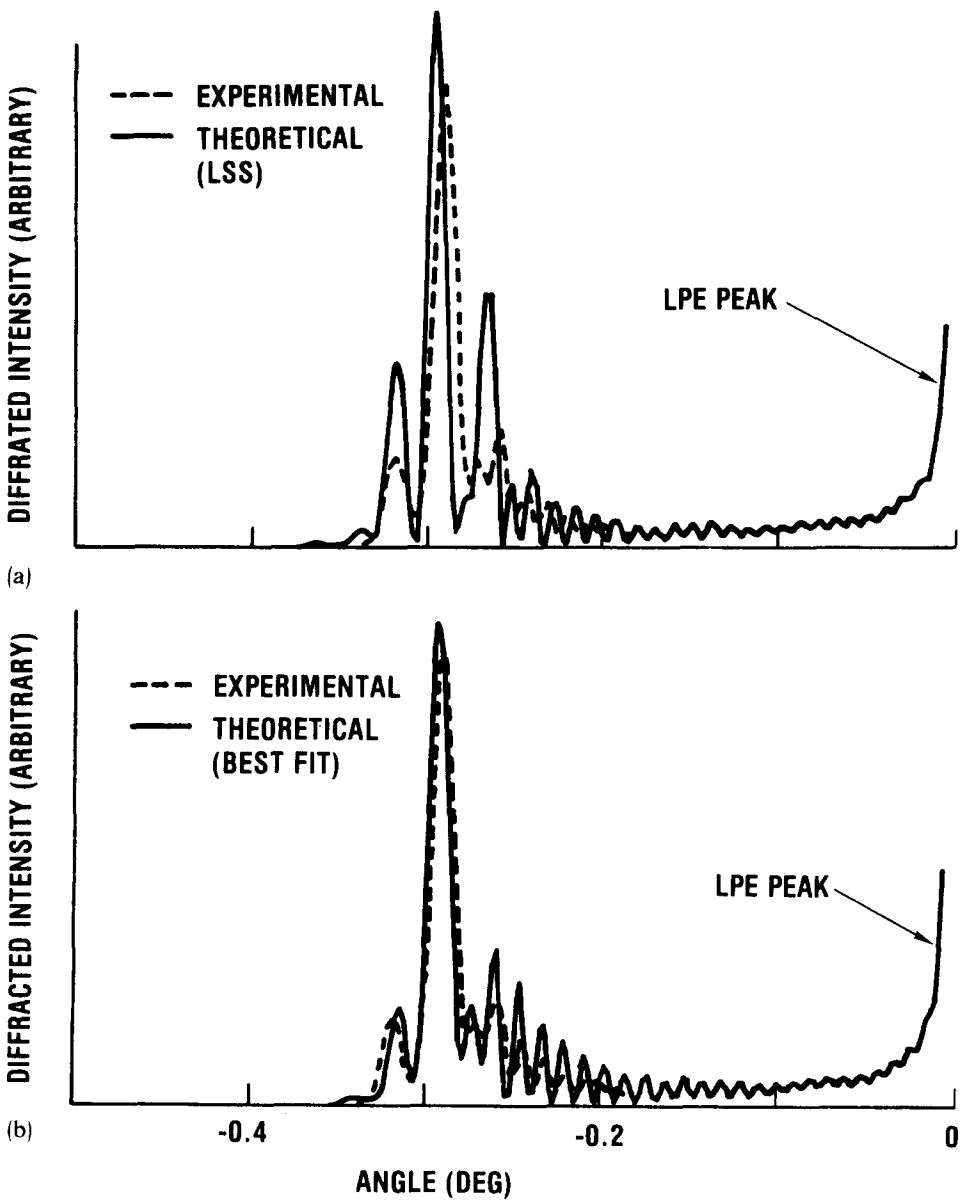


FIG. 9. Experimental (dashed) and theoretical (solid) diffracted x-ray intensity (arbitrary units) as a function of angle (deg) relative to the peak from the LPE bubble material (at 0°). The theoretical curve in (a) was calculated using the model (solid) strain distribution shown in Fig. 8, while the curve in (b) was calculated using the adjusted distribution (dots) in Fig. 8.

0.108 $\mu$m, $-1.1$, 7) was chosen to give an overall depth of 0.4 $\mu$m, and the dosage $8\times10^{14}$ ions/cm$^2$ was selected to give an average uniform strain of about 1%. A second 70-keV implant (0.140 $\mu$m, 0.060 $\mu$m, $-0.6$, 5) was chosen so that ${}^1R_p - {}^2R_p = \frac{3}{2}({}^1\sigma_p + {}^2\sigma_p)$, and the dosage $3\times10^{14}$ ions/cm$^2$ was adjusted to give the same peak strain. Within the implanted layer ($x < 0.4$ $\mu$m) the average strain has the desired uniform value, $1.07 \pm 0.09\%$.

The x-ray diffraction curve obtained from a double $B^+$ implant made according to these specifications is shown as a dashed curve in Fig. 9(a), and repeated in Fig. 9(b). Most of the diffracted intensity is concentrated in a narrow region between $-0.26°$ and $-0.32°$ which indicates that the strain in the implanted layer is indeed quite uniform. The solid curve in Fig. 9(a) is the theoretical x-ray diffraction curve calculated using the strain distribution predicted by the model, the solid curve in Fig. 8. The theoretical curve is in good qualitative agreement with the data, but the position of the main peak is slightly too low and the amplitudes of the first two side lobes are too high. By slightly modifying the distribution to the one indicated by ● in Fig. 8, it was found that much better agreement could be achieved as can be seen in Fig. 9(b). It must be emphasized that the changes shown in Fig. 8, being at most 0.09% strain, are well within the accuracy of the model as indicated by previous examples.

## CONCLUSIONS

The detailed properties of strain distributions in magnetic bubble materials have been modeled for by calculating the nuclear energy loss as a function of depth. The characteristic shape produced by a single implant—nonzero at the surface, rising to a peak near the average ion range, and then falling rapidly to zero—results from the increase in the nuclear energy loss rate $N$ with increasing depth (decreasing ion energy) combined with a decrease in the number of penetrating ions. For fixed incident energy, it was verified that the strain at any depth is proportional to the total dosage. When the incident energy is decreased, the depth of the distribution decreases, as expected, but it was also found that the strain increases at each point owing to an increase in $N$. Even though the dosage required to produce a given overall strain varied by two orders of magnitude for the three species investigated ($Ne^+$, $B^+$, $He^+$), the constant of proportionality between strain and nuclear energy loss density was roughly the same for all three ions, $K = 0.016 \pm 0.003$ (eV/Å$^3$)$^{-1}$. In cases of multiple implantation, the nuclear energy loss contributions from each component are additive, even when they involve different species. Finally, it was demonstrated that this model is sufficiently accurate ($\pm$ 10% relative error) to predict strain distributions resulting from multiple implantation and can be used as a guide in selecting the implantation conditions required for magnetic bubble devices.


[1] R. Wolfe, J. C. North, W. A. Johnson, R. R. Spiwak, L. J. Varnerin, and R. F. Fischer, AIP Conf. Proc. **10**, 339 (1973).
[2] J. C. North and R. Wolfe, in *Ion-Implantation in Semi-Conductors and Other Materials*, edited by B. L. Crowder (Plenum, New York, 1973).
[3] For a review, see D. K. Brice, in *Ion-Implantation in Semi-Conductors and Other Materials*, edited by B. L. Crowder (Plenum, New York, 1973).
[4] J. Lindhard, M. Scharff, and H. E. Schiott, Kgl. Danske Videnskab. Selskab, Mat.-Fys. Medd. **33**, (1963).
[5] K. Ju, R. O. Schwenker, and H. L. Hu, IEEE Trans. **MAG-15**, 1658 (1979).
[6] J. F. Gibbons, W. S. Johnson, and S. W. Mylorie, *Projected Range Statistics*, 2nd ed. (Halstead, New York, 1975).
[7] V. S. Speriosu, H. L. Glass, and T. Kobayashi, Appl. Phys. Lett. **34**, 539 (1979).
[8] V. S. Speriosu, H. L. Glass, and T. Kobayashi, presented at the Third International Conference on Magnetic Bubbles, Indian Wells, Calif., 1979 (unpublished).
[9] V. S. Speriosu, B. E. MacNeal, and H. L. Glass, presented at the IEEE International Magnetics Conference, Boston, Mass., 1980 (unpublished).
[10] See, for example, M. G. Kendall and A. Stuart, *The Advanced Theory of Statistics* (Hafner, New York, 1958).
[11] W. K. Hofker, D. P. Oosterhoek, N. J. Koeman, and H. A. M. DeGrefte, Radiat. Eff. **24**, 223 (1975).